Research Article | Vol. 27, No. 1 | 7 Jan 2019 | OPTICS EXPRESS 185
Optics EXPRESS

X-ray zoom lens allows for energy scans in X-ray microscopy

E. KORNEMANN,[1,*] T. ZHOU,[2] O. MÁRKUS,[1] A. OPOLKA,[1] T. U. SCHÜLLI,[2] J. MOHR,[1] AND A. LAST[1]

[1]*Institute of Microstructure Technology (IMT), Karlsruhe Institute of Technology (KIT), Hermann-von-Helmholtz-Platz 1 76344, Eggenstein-Leopoldshafen, Germany*
[2]*ESRF - The European Synchrotron Radiation Facility, 71 Avenue des Martyrs 38043, Grenoble, France*
[*]*elisa.kornemann@kit.edu*

Abstract: We introduce a new design and development of a compound refractive X-ray zoom lens for energy scans in X-ray microscopy. Energy scans are, in principle, equivalent to radial scans in the reciprocal space for X-ray diffraction. Thanks to the absence of sample or detector motions, energy scans are better suited for microscopy, which requires high stability. In addition, close to the absorption edge of an element, energy scans can yield chemical information when coupled with resonant effects in either full field diffraction X-ray microscopy (FFDXM) or X-ray absorption near edge structure (XANES) microscopy. Here, we demonstrate the concept by using a customized compound refractive X-ray zoom lens for 11 keV near the Ge K_α-edge. The working distance and magnification were kept constant during the energy scans by adapting the lens composition on switchable zoom lens fingers. This alleviates the need to reposition the lens while changing the energy and makes quantitative analysis more convenient for FFDXM. The fabricated zoom lens was characterized and proven suitable for the proposed measurement.

1. Introduction

Plenty new experimental ideas can become possible if one overcomes the chromatic nature of compound refractive lenses (CRLs) with the development of adaptive optics. As a compact, easy to use and inexpensive replacement for the bulky KB mirrors, this is in particular interesting for full field X-ray microscopy. One such idea is to replace the reciprocal space radial scans with energy scans using lenses with adjustable focal length. The latter has the advantage of enhanced stability and reproducibility as it eliminates the alignment errors caused by motor motions, motor vibrations and the sphere of confusion of diffractometers. Such idea has been demonstrated in the past, mostly using chromatic optics. A formalism for three-dimensional (3D) Bragg X-ray coherent diffraction imaging (BCDI) without sample movement was implemented [1] by scanning the energy of the incident beam. A similar energy scan has been used in 3D micro- and nano-focused X-ray diffraction to probe the reciprocal-space maps of a single SiGe island around the Si (004) Bragg peak [2]. The drawback of using chromatic optics in these cases are the constant readjustments of the lens-sample distance and the additional corrections during data analysis. Nevertheless, performing energy scans is, in cases where sample movement is forbidden, the ideal and the only solution to probe the reciprocal space.

Scanning in small energy steps around the absorption energy of an element can reveal additional chemical information about the sample, this is known as resonant scattering for diffraction and X-ray absorption near edge structure (XANES) for absorption experiments. The combination of anomalous and coherent diffraction has already been used to map both strain and composition fields inside core-shell nanoparticles [3]. This approach is to be further extended at the Full Field Diffraction X-ray Microscopy (FFDXM) setup on the ID01 beamline at the European Synchrotron Radiation Facility (ESRF). FFDXM naturally yields lattice strain

#349862 https://doi.org/10.1364/OE.27.000185
Journal © 2019 Received 9 Nov 2018; revised 9 Dec 2018; accepted 10 Dec 2018; published 3 Jan 2019

Optics EXPRESS

and tilt information on an area larger than 100 µm x 100 µm at the sample surface with 200 nm resolution (line and space). By coupling with resonant scattering, information on the chemical composition of the anomalous element can be further obtained.

To achieve this, the microscopy setup has to be changed from a chromatic CRL to an objective with variable focal length, which can easily be included into the existing experimental setup. The recently introduced X-ray zoom lens [5,6] can keep a fixed working distance and constant magnification factor over a required energy range. This X-ray zoom lens consists of SU-8 lens elements fabricated by deep X-ray lithography [7–9] and positioned on bendable zoom lens fingers. The focal length can be adjusted by bending lens elements in or out of the beam path. This X-ray optics is a comparably cheap solution and is used with a customized lens layout in this new experimental setup.

2. Optical setup and X-ray zoom lens layout

For demonstration, the target energy of 11.103 keV was selected for the X-ray zoom lens. This energy corresponds to the Ge-K_α-edge found in isolated compositionally graded SiGe pillars, which were previously studied with the K-map technique at ID01 [4]. To correctly apply the scheme of multi-wavelength anomalous X-ray scattering [10], it is necessary to measure several data points close to the Ge-K_α-edge in energy steps of 5 eV and additionally two data points 50 eV far away from the edge. The customized X-ray zoom lens has one configuration for each of these energies to achieve FFDXM imaging with a fixed working distance and a constant magnification. The experimental setup for this demonstration is shown in Fig. 1. The sample distance s_d is defined from the sample plane to the first edge of the first finger of the X-ray zoom lens at position z = 0. The z-direction is defined along the optical axis. The working distance w_d is defined from the first edge of the first zoom lens finger of the X-ray zoom lens (z = 0) to the detector plane with w_d = 6.5 m. The CRL's maximum length is L_{CRL} = 61 mm.

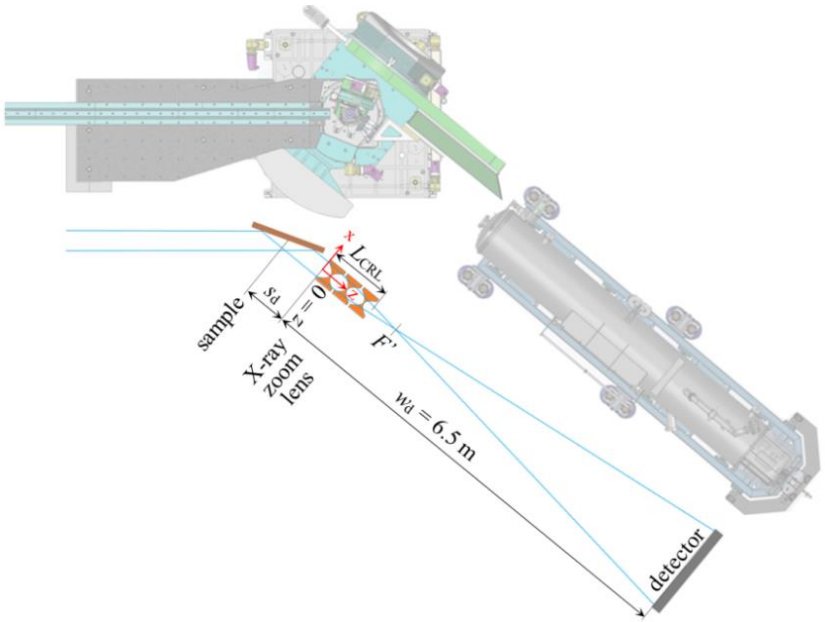

Fig. 1. A CAD model of the FFDXM in situ setup at ID01, ESRF (top), with a sketch of optical path through the sample in Bragg-condition, objective (X-ray zoom lens), and detector (bottom). z = 0 is defined to be at the first edge of the first zoom lens finger. The sample distance s_d is the distance from the sample plane to z = 0 and the working distance w_d is the distance from the detector plane from z = 0.

Optics EXPRESS

The detector is an Andor Zyla 4.2 PLUS sCMOS camera with 2160 x 2560 active pixels and pixel size p_{CMOS} = 6.5 µm. For quantitative analysis, it is essential that the magnification is kept constant for all photon energies. To achieve a desirable resolution of σ_{min} = 400 nm per line and space, the magnification factor was set to M ~65:

$$M = \frac{4\, p_{CMOS}}{\sigma_{min}}. \tag{1}$$

The factor four takes into account that four detector pixels are needed to resolve a pair of line and space as indicated by the Nyquist-Shannon sampling theorem [11]. With these requirements the sample distance s_d and characteristics of the X-ray zoom lens can be calculated for the photon energies around the absorption edge at a fixed working distance w_d = 6.5 m. Because the sample and the detector positions are fixed during the energy scan, the objective has to be adapted by changing its characteristics to keep the back focal point F' at a fixed position [see Fig. 2].

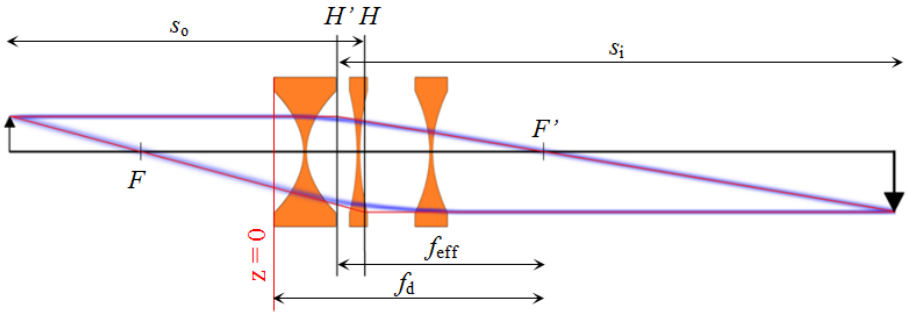

Fig. 2. X-ray lens system with optical path of two simulated rays (blue), labeled parameters and constructed (red rays) principle plains H and H'.

For a CRL made of identical and equidistant elements with overall length L_{CRL}, radius of curvature in the apex of the parabola R, δ the decrement of the refractive index and N lens elements, the focal length f can be approximated by [12,13]

$$f = \frac{R}{2\delta N} + \frac{L_{CRL}}{6}. \tag{2}$$

To achieve fixed working distance for very small energy step size of 5 eV, the new zoom lens was designed with lens elements having a slightly different radii R, resulting in non-equidistant lens elements like in Fig. 2. Consequently, the approximation (2) is here replaced by raytracing. The effective focal length f_{zl} is defined from the back principle plane H' of the lens system to the back focal point F' [14]. The refractive index n of any material is slightly below one in the X-ray regime and in general denoted as:

$$n = 1 - \delta + i\beta. \tag{3}$$

Here, β is the absorption coefficient and δ the decrement of the refractive index. For the X-ray zoom lenses, we used a SU-8 resist (type "mr-X-50" from micro resist technology GmbH, Berlin) and measured δ for photon energies E_{Ph} for a 400 µm thick resist ranging from 8.7 keV to 40 keV. The value of the absorption coefficient δ for the desirable energy range can be approximated by:

$$\delta = \frac{0.00027142}{(E / \mathrm{keV})^2} \tag{4}$$

Optics EXPRESS

with a tolerance below 1%. For E_{Ph} = 11.103 keV δ is $2.202 \cdot 10^{-6}$. The absorption coefficient β can be found in the literature [15]. The object distance s_o from the sample to the front principle plane is calculated by the image distance s_i from detector towards the back principle plane and the magnification factor M [see Fig. 2]:

$$s_o = \frac{s_i}{M}. \tag{5}$$

The sample distance was determined as s_d = 67.5 mm using Eq. (5) and the specific lens element positions on the zoom lens fingers [see Fig. 4]. The X-ray zoom lens was optimized in a way that the distances s_d and w_d stay constant when changing the photon energy. Therefore, the focal length of the zoom lens was adapted accordingly.

Deep X-ray lithography allows for the manufacturing of 1D line focussing refractive lenses. A point focus requires a 2D-lens and therefore two line focus lenses are mounted perpendicular to each other rotated around the optical axis [see Fig. 3].

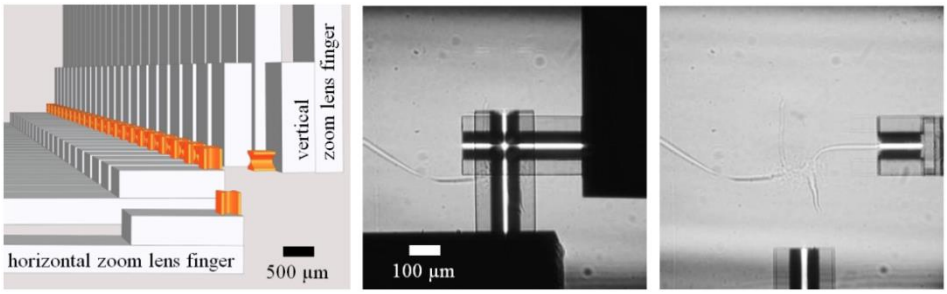

Fig. 3. X-ray zoom lens as a CAD drawing (left) with the first (front) zoom lens fingers with horizontal and vertical focusing lens element (orange) moved out of the beam path and all other zoom lens fingers positioned in the beam for a point focus lens. Radiographs at 11 keV of the X-ray zoom lens with six lens elements of each direction aligned in the beam (middle) and all lens elements moved out of the beam (right).

For small energy steps such as 5 eV, it is technically unfeasible to vary the number of lens elements in the beam. Instead, the fixed working distance is achieved by exchanging lens elements by elements with slightly different radii. Nine different zoom lens configurations have been realized in total, for FFDXM measurement at nine energies around the Ge K_α-edge [see Table 1]. Only configurations that are symmetrical in relation to the lens center of the zoom lens [see Fig. 4] were used to keep the position of the principle planes and hence the magnification M as constant as possible. The focal length varies slightly for each configuration, as it depends also on the length of the CRL L_{CRL} [see Eq. (1)]. The latter becomes larger as lens elements far away from the center are switched in. The optimized zoom lens layout is shown in Fig. 4. All lens elements in the current zoom lens layout have an aperture of A = 98 µm and radii between R = 7.050 µm and 8.305 µm. The variation of the radius for neighboring lens elements is in average ΔR ~150 nm. Overall N = 66 1D lens elements are manufactured on 22 zoom lens fingers, respectively for the horizontal and vertical focusing half lens [see Fig. 4].

In each configuration six horizontal and vertical zoom lens fingers are placed in the beam. The total number of lens elements in the beam is thus N = 18 for each focusing direction. The average transmission for the configurations is (20.2 ± 0.2)%. The radii of horizontal and corresponding vertical lens elements are slightly different to compensate for the astigmatism originated from the shifted lens element positions. As a result, the back focal point F' is slightly different for horizontal and vertical direction. The configuration #5 for the photon energy at the Ge K_α-edge is shown in Fig. 4 (green highlighted). The selected six zoom lens fingers are v05, v10-v13, v18 for the vertical focusing half lens and h05, h10-h13, h18 for the horizontal focusing half lens. All other zoom lens fingers are kept out of the beam path for this configuration.

Optics EXPRESS

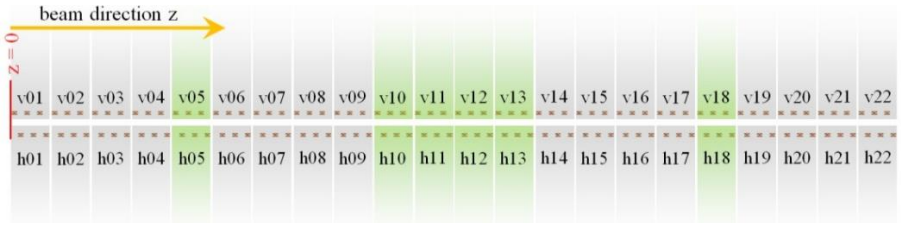

Fig. 4. X-ray zoom lens layout for the energy scan with FFDXM at nine different energies around the Ge K_α-edge. There are 22 zoom lens fingers (shown as grey and green stripes), respectively, for the horizontal focusing lens elements (h01-h22) and the vertical focusing lens elements (v01-v22). In each configuration, six zoom lens fingers with overall N = 18 lens elements are positioned in the beam path, for vertical and horizontal direction, respectively. The configuration #5 for the exact photon energy at the Ge K_α-edge of $E_{\mathrm{Ph\_GeK}}$ = 11.103 keV is highlighted in green.

Table 1 shows all parameters of the optimized X-ray zoom lens for all nine energies (seven with 5 eV step size and two with 50 eV step size). "X" marks zoom lens fingers that are positioned in the beam and "o" marks zoom lens fingers that are moved out of the beam path [see Table 1, column 5]. Note that while the X-ray zoom lens can also be optimized to achieve a constant effective focal length f_{zl} (i.e., the distance from the back principle plane H' to the back focal point F' [Fig. 2]), in the microscopy setup, the goal is to achieve a constant magnification factor M. To emphasize this effect, Table 2 shows exemplarily the effect on M when the configuration of the X-ray zoom lens is kept constant (e.g., config. #5). For an energy step of 50 eV, for instance, to get a sharp image in the detector plane, one would have to move the detector up to Δw_{d} = 8.5 m.

Table 1. Parameters of nine optimized X-ray zoom lens configurations for energy scans with FFDXM around Ge K_α-edge at 11.103 keV (config. #5). Sample distance s_{d} and working distance w_{d} are kept constant during energy scan, resulting in nearly constant effective focal length f_{zl} and magnification M.

# config.	E_{Ph} / keV	s_{d} / mm	$w_{\mathrm{d\_hor/ver}}$ / m	Configuration of X-ray zoom lens: X = zoom lens finger in beam; o = zoom lens finger out of beam	M_{hor}	M_{ver}	$f_{\mathrm{zl\_hor}}$ / mm	$f_{\mathrm{zl\_ver}}$ / mm	$\Delta f_{\mathrm{zl\_hor}}$ / %	$\Delta f_{\mathrm{zl\_ver}}$ / %
1	11.053	67.5	6.5	XoooooooXXXXooooooooX	65.2	65.0	97.7	98.1	0.89	0.87
2	11.088	67.5	6.5	oXoooooooXXXXoooooooXo	65.4	65.2	97.4	97.8	0.63	0.61
3	11.093	67.5	6.5	ooXoooooooXXXXooooooXoo	65.6	65.3	97.2	97.6	0.39	0.38
4	11.098	67.5	6.5	oooXoooooXXXXooooooXooo	65.7	65.4	97.0	97.4	0.18	0.17
5	**11.103**	**67.5**	**6.5**	**ooooXoooooXXXXooooXoooo**	**65.8**	**65.6**	**96.8**	**97.2**	**0.00**	**0.00**
6	11.108	67.5	6.5	ooooooXoooXXXXoooXoooooo	65.9	65.7	96.7	97.1	-0.15	-0.14
7	11.113	67.5	6.5	oooooooXooXXXXooXooooooo	66.0	65.7	96.6	97.0	-0.26	-0.26
8	11.118	67.5	6.5	ooooooooXoXXXXoXoooooooo	66.1	65.8	96.5	96.9	-0.35	-0.35
9	11.153	67.5	6.5	oooooooooXXXXXXoooooooo	66.1	65.8	96.4	96.8	-0.42	-0.41

Optics EXPRESS

Table 2. Parameters for configuration #5 of the X-ray zoom lens for the energy scan with FFDXM around the Ge K$_\alpha$-edge at 11.103 keV. Sample distance s_d stays constant during the energy scan. This static CRL objective yields a nearly constant effective focal length f_{zl}, but the working distance w_d and magnification M change drastically.

# config.	E_{Ph} / keV	s_d / mm	w_{d_hor} / m	w_{d_ver} / m	Configuration of X-ray zoom lens: X = zoom lens finger in beam; o = zoom lens finger out of b.	M_{hor}	M_{ver}	f_{zL_hor} / mm	f_{zL_ver} / mm	Δf_{zL_hor} / %	Δf_{zL_ver} / %
1	11.053	67.5	4.14	4.15	ooooXooooXXXXooooXoooo	41.8	41.7	96.0	96.4	-0.85	-0.85
2	11.088	67.5	5.55	5.56	ooooXooooXXXXooooXoooo	56.2	56.0	96.6	97.0	-0.25	-0.25
3	11.093	67.5	5.84	5.84	ooooXooooXXXXooooXoooo	59.1	58.9	96.7	97.0	-0.17	-0.17
4	11.098	67.5	6.15	6.15	ooooXooooXXXXooooXoooo	62.3	62.0	96.7	97.1	-0.08	-0.08
5	**11.103**	**67.5**	**6.50**	**6.50**	**ooooXooooXXXXooooXoooo**	**65.8**	**65.6**	**96.8**	**97.2**	**0.00**	**0.00**
6	11.108	67.5	6.89	6.89	ooooXooooXXXXooooXoooo	69.8	69.5	96.9	97.3	0.08	0.08
7	11.113	67.5	7.33	7.33	ooooXooooXXXXooooXoooo	74.3	74.0	97.0	97.4	0.17	0.17
8	11.118	67.5	7.83	7.83	ooooXooooXXXXooooXoooo	79.4	79.0	97.1	97.5	0.25	0.25
9	11.153	67.5	15.0	14.9	ooooXooooXXXXooooXoooo	151.9	150.7	97.7	98.0	0.85	0.85

3. Fabrication of customized X-ray zoom lens

The X-ray zoom lens consists of lens elements of SU-8 polymer resist, which is cross-linked during deep X-ray lithography exposure at a synchrotron source. The material is radiation stable up to a deposited dose of at least 2 MJ/cm^3 [16,17]. With deep X-ray lithography all refractive lens elements are fabricated well aligned in one step. The mandatory X-ray absorber mask is written with an electron beam writer with a spot size of 8 nm diameter [18]. The length of one lens element L_{lens} along the optical axis is the sum of two parabolas and the web in between. With a web size of w = 7 µm and an aperture of A = 98 µm the length of a lens is calculated by:

$$L_{lens} = w + 2\left(\frac{A^2}{8R}\right). \tag{6}$$

The smallest variation in the radius of curvature in this layout is ΔR = 8 nm. Therefore, the change in the length of lens elements with an average radius of curvature in the apex of parabola of R = 7.6 µm can be estimated by:

$$L_1 - L_2 = \frac{A^2}{4}\left(\frac{1}{R} - \frac{1}{R+\Delta R}\right) \approx \Delta R\left(\frac{A}{2R}\right)^2 \tag{7}$$

with $\Delta R \ll R$. It can be noted that the 8 nm writing spot size of the electron beam writer is equal to only ±2.4% of required change L_1-L_2 = 0.330 µm. This guaranties a precise and reliable fabrication of the X-ray zoom lens elements.

Two silicon stripes, each containing 66 lens elements, were glued to a zoom lens substrate providing the bending fingers [see Fig. 3 and Fig. 5]. Each zoom lens substrate with the glued silicon stripe was diced to form the 22 zoom lens fingers as shown in the layout [see Fig. 4]. These bendable zoom lens fingers were preloaded with a stainless steel bar as deadlock and held the lens elements at their free end [see Fig. 5 left]. For a point focus X-ray zoom lens two zoom lens substrates, one for vertical and one for horizontal focusing direction, are mounted perpendicular to each other rotated around the optical axis [see Fig. 3 and Fig. 5 right]. The achieved angular tolerance was 90°±0.06° by laser triangulation. Details of the construction,

Optics EXPRESS

mounting and precision of the lens elements as well as the electronic control of the X-ray zoom lens are explained elsewhere [5].

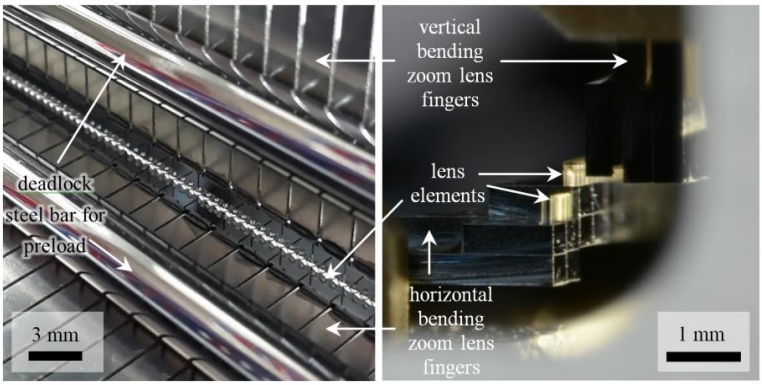

Fig. 5. X-ray zoom lens with customized lens layout for the energy scan in FFDXM. The lens elements are positioned on the free end of the bendable zoom lens fingers. The zoom lens fingers are preloaded with a stainless steel bar (left) for the precise positioning in the beam path. In the picture on the right the first two zoom lens fingers are bent out of the beam, all the other zoom lens fingers are positioned in the beam and the lens elements from both directions are crossing each other.

4. Optical characterization of X-ray zoom lens

At beamline ID01, ESRF the custom-designed X-ray zoom lens was characterized and tested. In Fig. 3 (middle and left) the radiograph at 11 keV of the aligned zoom lens is shown with the two crossed line focus lenses acting as a point focusing optics. The flat field, stopped down to 90 µm x 90 µm showed good homogeneity with only 12.5% intensity deviation for the average intensity. The quality of the fabricated lens was characterized with a series of ptychography scans on a Siemens-star test sample in transmission. With a 300 nm step size the sample is moved through the focused X-ray beam in an area of 10 µm x 10 µm. A far-field diffraction pattern was recorded with a MaxiPix 2x2 detector with 516 x 516 active pixels and pixel size of 55 µm at a distance of 102 cm. The illuminated object and the wave field probing the sample were reconstructed with PyNX.Ptycho [19].

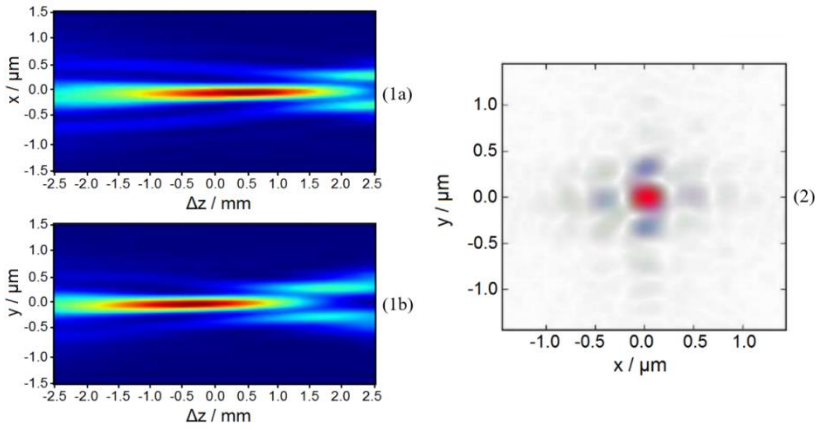

Fig. 6. Beam profiles of the X-ray zoom lens in configuration #5 at 11.103 keV showing the caustic focus profiles along the beam path in horizontal (1a) and vertical (1b) direction. Point focus is achieved as evidenced by the beam profile in the focal plane (2).

Optics EXPRESS

In Fig. 6 is shown the beam profiles of the X-ray zoom lens in configuration #5 at 11.103 keV. On the left side the caustic focus profiles are shown along the beam path in horizontal [Fig. 6(1a)] and vertical [Fig. 6(1b)] direction. The observed difference in the focal distance was by design, in order to compensate for the position shift of one lens element between the vertical and horizontal lenses [see also Fig. 7]. On the right side [Fig. 6(2)], a point focus was achieved as evidenced by the intensity distribution in the focal plane.

More ptychography measurements were carried out in different configurations and at different energies. In Table 3 are found the reconstructed focal distances f and focal spot sizes σ by ptychography compared to their theoretical values. All reconstructed focal distances f are defined as the distance from z = 0 to the back focal point F'; not to be confused with the effective focal length f_{ZL} as calculated in section 2 [Table 1 and Table 2]. The focal spot sizes shown in Fig. 7 were calculated using wavefront propagation [19]. On the left of Fig. 7, it was demonstrated that the focal point, horizontal or vertical, remained indeed constant despite changing the energy by switching to the corresponding configurations (#4, #5, and #9).

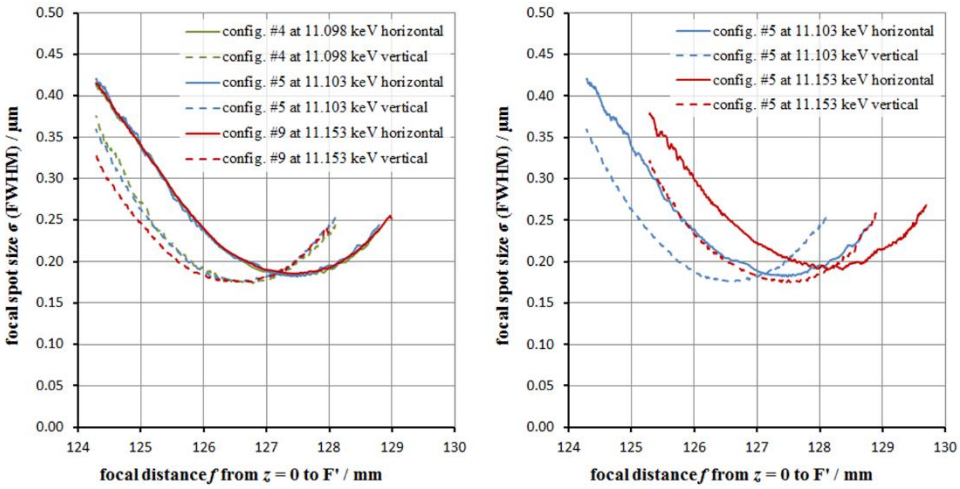

Fig. 7. Results of ptychography measurements of a point focus zoom lens at ESRF, ID01, with focal distances f and focal spot sizes σ in three configurations at their intended photon energy (left) and one configuration compared with its performance at 50 eV higher photon energy (right).

The simulated and measured focal distances f all showed the expected behavior regarding the astigmatism and required static focal point, with variations in the range of less than 0.1% [see Table 3, col. 3-7]. This validates the concept and functionality of the designed zoom lens. Focal spot sizes in the range of σ = 175 nm to 193 nm were obtained with an uncertainty of ~10%. The results are comparable to the calculated minimal focal spot sizes after taking into account the diffraction limit, source size and astigmatism [Table 3, col. 8-9] [5].

In a second approach, the difference between using a fixed chromatic lens and an adaptive zoom lens at different energies is shown. Ptychography measurements were performed for configuration #5 at its intended photon energy and at 50 eV above [see Fig. 7 right]. A shift of focal point of 0.8 mm was observed by operating at 50 eV above its intended energy. The shift was further confirmed by the simulated data [Table 4]. Such shift should be avoided as it introduces a change in the magnification M and blurs the FFDXM image. For the designed zoom lens, this was achieved by switching to the corresponding configuration #9.

Optics EXPRESS

Table 3. Comparison between the focal distances and focal spot sizes obtained by ptychography reconstructions and by simulations for the designed zoom lens. The result is shown for configurations #4, #5, #9 at their intended photon energy and for configuration #5 at 50 eV above its intended photon energy.

# config.	E_{Ph} / keV	horizontal focal distance f_H / mm *measured* (simulated)	vertical focal distance f_V / mm *measured* (simulated)	Δf_H measured - simulated *absolute* / mm and (relative / %)	Δf_V measured - simulated *absolute* / mm and (relative / %)	Astigmatism $\Delta(f_H\text{-}f_V)$ / mm *measured* (simulated)	horizontal focal spot size σ_H/ µm *measured* (calculated)	vertical focal spot size σ_V/ µm *measured* (calculated)
4	11.098	*127.377* (127.377)	*126.602* (126.589)	*0.000* (0.00)	*0.013* (0.01)	*0.775* (0.788)	*0.183* (0.167)	*0.176* (0.080)
5	11.103	*127.397* (127.372)	*126.650* (126.584)	*0.025* (0.02)	*0.066* (0.05)	*0.747* (0.788)	*0.182* (0.167)	*0.175* (0.080)
9	11.153	*127.406* (127.389)	*126.544* (126.601)	*0.017* (0.01)	*-0.057* (-0.04)	*0.862* (0.788)	*0.184* (0.167)	*0.175* (0.080)
5	11.153	*128.129* (128.209)	*127.488* (127.417)	*-0.080* (-0.06)	*0.071* (0.06)	*0.641* (0.792)	*0.193* (0.167)	*0.176* (0.080)

Table 4. Focal spot shift of a chromatic CRL compared to the adaptive X-ray zoom lens from ptychography reconstruction results and from simulated data.

	Δf_H at E_{Ph} (11.153 keV– 11.103 keV) for *static configuration #5 and* adapting zoom lens in configuration #9 and #5 absolute / mm and (relative / %)	Δf_V at E_{Ph} (11.153 keV– 11.103 keV) for *static configuration #5 and* adapting zoom lens in configuration #9 and #5 absolute / mm and (relative / %)
measured	*0.752 mm (0.59 %)* 0.029 mm (0.02 %)	*0.886 mm (0.69 %)* -0.058 mm (-0.05 %)
simulated	*0.832 mm (0.65 %)* 0.012 mm (0.01 %)	*0.828 mm (0.65 %)* 0.012 mm (0.01 %)

In a last approach, the designed X-ray zoom lens was used as imaging optics for the FFDXM setup in a transmission mode. A test pattern was positioned at distance s_d = (67 ± 1) mm upstream of the lens. Two sets of slits with 0.3 mm opening upstream of the sample were used to define the aperture of the zoom lens. The detector was placed downstream of the zoom lens with w_d = 6.5 m. The magnification was therefore M ~65. A series of images was taken to estimate the resolution of the zoom lens with different configurations and at different energies. In Fig. 8 the entire test structure was imaged with the X-ray zoom lens (FoV = 86 µm x 86 µm) in configuration #6 at E_{Ph} = 11.103 keV [Fig. 8. top left]. A detailed view shows the smallest structures resolved [Fig. 8, top right]. At the bottom of Fig. 8 are shown three images taken with Fig. 8(a) configuration #6 at its intended energy 11.103 keV and Fig. 8(b) configuration #9 at its intended energy 11.148 keV. Both show equal imaging quality, the 150 nm lines are resolved. Figure 8(c) is taken in configuration #6, but at the energy 11.148 keV, thus out of focus. Compared to Fig. 8(b), Fig. 8(c) shows broadened stripes between the structured fields and significant edge effects, which indicates the out of focus position of the lens. The 100 nm lines are not resolvable as they are under-sampled with only two pixels per line and space in the detector plane. With the adaptive zoom lens, the measured change in the magnification (by comparing results from Figs. 8(a) and 8(b)) is 35% smaller compared to the expected change for a chromatic CRL (by comparing results from Figs. 8(a) and 8(c)). The images of the test pattern also confirmed that the desired resolution of σ_{min} = 400 nm per line and space was

Optics EXPRESS

reached for the current zoom lens. This microscopy setup was restricted by the detector resolution. Taking the the ptychography scan results with a measured focal spot size of σ ~180 nm into account, a resolution of 350 nm line and space is achievable with this X-ray zoom lens.

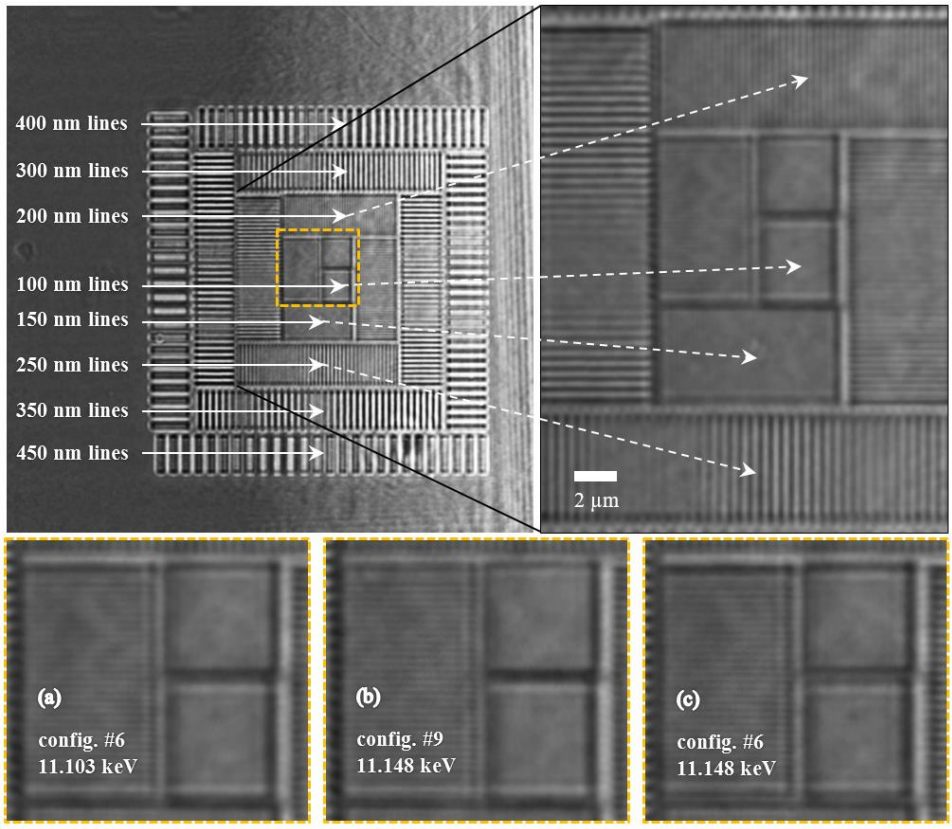

Fig. 8. Test pattern with vertical and horizontal line structures of different sizes imaged by the X-ray zoom lens with a FoV of 86 µm x 86 µm in configuration #6 at E_{Ph} = 11.103 keV (top left). A more detailed view is shown (top right) for the smallest resolvable structures. On the bottom are shown a comparison between three images taken with (a) configuration #6 its intended energy and (c) 45 eV above, and (c) configuration #9 at its intended energy.

5. Conclusion

A customized compound refractive X-ray zoom lens has been designed and realized for energy scans in diffraction X-ray microscopy. The X-ray zoom lens, which consists of SU-8 lenses fabricated by deep X-ray lithography, has been tested and characterized at ID01, ESRF. The working distance and the magnification factor of this zoom lens, to be used as objective in the microscopy setup, are kept constant for nine energies around the Ge K_α-edge by switching to the corresponding configuration. Hence, there is no sample, objective or detector motion involved during energy scans, the images are kept sharp in microscopy mode and the magnification constant in shadow projection mode. The concept was validated by ptychography and full field microscopy. The ptychography showed that a fixed working distance was achieved at the intended energies with a measured focal spot sizes of σ = (180 ± 18) nm. Additionally, the imaging of line test structures showed an intended resolution of 400 nm line and space on a FoV of 86 µm x 86 µm. The resolution is assumed to be around 350 nm, but was restricted by the detector resolution. The result shows the potentials of such X-ray zoom lens for energy scans

Optics EXPRESS

to eliminate sample movement in nano-focused, full field X-ray diffraction and absorption microscopy. The detailed description and analysis of the experiment with SiGe pillars at ID01 shall be described in a separate publication.

Funding

Helmholtz Association (Karlsruhe Nano Micro Facility, KNMF); Karlsruhe School of Optics & Photonics (KSOP).

Acknowledgments

The authors thank the ESRF for providing beam time at ID01. We thank the Karlsruhe Nano Micro Facility (KNMF), a research infrastructure in the Helmholtz association for the possibility to fabricate the polymer X-ray lenses by deep X-ray lithography. We further thank Vincent Favre Nicolin for discussions regarding the ptychography reconstruction.

References

1. W. Cha, A. Ulvestad, M. Allain, V. Chamard, R. Harder, S. J. Leake, J. Maser, P. H. Fuoss, and S. O. Hruszkewycz, "Three dimensional variable-wavelength x-ray bragg coherent diffraction imaging," Phys. Rev. Lett. **117**(22), 225501 (2016).
2. T. W. Cornelius, D. Carbone, V. L. R. Jacques, T. U. Schülli, and T. H. Metzger, "Three-dimensional diffraction mapping by tuning the X-ray energy," J. Synchrotron Radiat. **18**(Pt 3), 413–417 (2011).
3. S. T. Haag, M.-I. Richard, S. Labat, M. Gailhanou, U. Welzel, E. J. Mittemeijer, and O. Thomas, "Anomalous coherent diffraction of core-shell nano-objects: A methodology for determination of composition and strain fields," Phys. Rev. B Condens. Matter Mater. Phys. **87**(3), 035408 (2013).
4. M. Meduňa, F. Isa, A. Jung, A. Marzegalli, M. Albani, G. Isella, K. Zweiacker, L. Miglio, and H. von Känel, "Lattice tilt and strain mapped by X-ray scanning nanodiffraction in compositionally graded SiGe/Si microcrystals," J. Appl. Cryst. **51**(2), 368–385 (2018).
5. E. Kornemann, O. Márkus, A. Opolka, T. Zhou, I. Greving, M. Storm, C. Krywka, A. Last, and J. Mohr, "Miniaturized compound refractive X-ray zoom lens," Opt. Express **25**(19), 22455–22466 (2017).
6. E. Kornemann, O. Márkus, A. Opolka, K. Sawhney, A. Cecilia, M. Hurst, T. Baumbach, A. Last, and J. Mohr, "Optical Characterization of an X-ray Zoom Lens," Microsc. Microanal. **24**(S2), 268–269 (2018).
7. Y. Ohishi, A. Q. R. Baron, M. Ishii, T. Ishikawa, and O. Shimomura, "Refractive x-ray lens for high pressure experiments at SPring-8," Nucl. Instrum. Methods Phys. Res. A **467–468**, 962–965 (2001).
8. F. Marschall, A. Last, M. Simon, M. Kluge, V. Nazmov, H. Vogt, M. Ogurreck, I. Greving, and J. Mohr, "X-ray full field microscopy at 30 keV," J. Phys. Conf. Ser. **499**, 012007 (2014).
9. E. Reznikova, T. Weitkamp, V. Nazmov, M. Simon, A. Last, and V. Saile, "Transmission hard x-ray microscope with increased view field using planar refractive objectives and condensers made of SU-8 polymer," J. Phys. Conf. Ser. **186**, 012070 (2009).
10. H. Renevier, J. Coraux, M. G. Proietti, V. Favre-Nicolin, and B. Daudin, "Multiwavelength anomalous diffraction (MAD) and diffraction anomalous fine structure (DAFS) in the study of structural properties of nanostructures," Acta Crystallogr. A **63**(a1), 63 (2007).
11. R. J. Marks II, *Introduction to Shannon Sampling and Interpolation Theory* (Springer, 1991).
12. V. G. Kohn, I. Snigireva, and A. Snigirev, "Diffraction theory of imaging with X-ray compound refractive lens," Opt. Commun. **216**(4-6), 247–260 (2003).
13. V. G. Kohn, "An exact theory of imaging with a parabolic continuously refractive x-ray lens," J. Exp. Theor. Phys. **97**(1), 204–215 (2003).
14. E. Hecht, *Optics / Eugene Hecht* (Addison-Wesley, 2002), Chap. 5&6.
15. E. Gullikson, "Index of refraction," http://henke.lbl.gov/optical_constants/getdb2.html.
16. V. Nazmov, E. Reznikova, J. Mohr, A. Snigirev, I. Snigireva, S. Achenbach, and V. Saile, "Fabrication and preliminary testing of X-ray lenses in thick SU-8 resist layers," Microsyst. Technol. **10**(10), 716–721 (2004).
17. A. Snigirev, I. Snigireva, M. Drakopoulos, V. Nazmov, E. Reznikova, S. Kuznetsov, M. Grigoriev, J. Mohr, and V. Saile, "Focusing properties of X-ray polymer refractive lenses from SU-8 resist layer," Proc. SPIE **5195**, 21 (2003).
18. KNMF Laboratory for Micro- and Nanostructuring, "Electron Beam Lithography," https://www.knmf.kit.edu/downloads/KNMF_Technology_Description_1_IMT_EBL.pdf
19. O. Mandula, M. Elzo Aizarna, J. Eymery, M. Burghammer, and V. Favre-Nicolin, "PyNX.Ptycho: a computing library for X-ray coherent diffraction imaging of nanostructures," J. Appl. Cryst. **49**(5), 1842–1848 (2016).